


Atmospheric turbulent structures and fire sweeps during shrub fires and implications for flaming zone behaviour

Marwan Katurji^{A,*}, Bob Noonan^A, Jiawei Zhang^{A,B} , Andres Valencia^C, Benjamin Shumacher^{A,D} , Jessica Kerr^B, Tara Strand^C, Grant Pearce^{B,E}  and Peyman Zawar-Reza^A

For full list of author affiliations and declarations see end of paper

***Correspondence to:**

Marwan Katurji
School of Earth and Environment,
University of Canterbury, New Zealand
Email: marwan.katurji@canterbury.ac.nz

ABSTRACT

Background. Wildfires propagate through vegetation exhibiting complex spread patterns modulated by ambient atmospheric wind turbulence. Wind gusts at the fire-front extend and intensify flames causing direct convective heating towards unburnt fuels resulting in rapid acceleration of spread. **Aims.** To characterise ambient and fire turbulence over gorse shrub and explore how this contributes to fire behaviour. **Methods.** Six experimental burns were carried out in Rakaia, New Zealand under varying meteorological conditions. The ignition process ensured a fire-line propagating through dense gorse bush (1 m high). Two 30-m sonic anemometer towers measured turbulent wind velocity at six different levels above the ground. Visible imagery was captured by cameras mounted on uncrewed aerial vehicles at 200 m AGL. **Key results.** Using wavelet decomposition, we identified different turbulent time scales that varied between 1 and 128 s relative to height above vegetation. Quadrant analysis identified statistical distributions of atmospheric sweeps (downbursts of turbulence towards vegetation) with sustained events emanating from above the vegetation canopy and impinging at the surface with time scales up to 10 s. **Conclusions.** Image velocimetry enabled tracking of ‘fire sweeps’ and characterised for the first time their lifetime and dynamics in comparison with overlying atmospheric turbulent structures. **Implications.** This methodology can provide a comprehensive toolkit when investigating coupled atmosphere–fire interactions.

Keywords: coherent structures, fire sweeps, fire turbulence, fire–atmosphere interactions, flaming zone, image velocimetry, surface-layer turbulence, UAV.

Introduction

Turbulence is a ubiquitous property of the Atmospheric Boundary Layer (ABL) that extends up to 1–2 km above ground level (AGL). ABL turbulence modulates how the near-surface atmosphere interacts with the additional energy perturbations caused by wildland fires over timescales from seconds to hours (Stull 1988). Closer to the surface, turbulent processes control heat, momentum and moisture transport between vegetated surfaces and the overlying Atmospheric Surface Layer (ASL). The ASL extends between 100 and 200 m above the surface and is strongly influenced by wind shear associated with surface drag producing mechanically induced turbulence (LeMone *et al.* 2019). Wildland fires produce positively buoyant turbulent motion that when coupled with overlying cooler air can lead to significant downward surges of momentum, interacting with ASL turbulence and potentially modulating a fire’s rate of spread over short periods of time (Cunningham and Linn 2007; Sun *et al.* 2009; Heilman *et al.* 2019). Identifying these processes from observations and studying their characteristics leading to coupled fire–atmosphere induced dynamics will help develop and evaluate new theories on how atmospheric turbulence interacts with wildland fires (Bebieva *et al.* 2020).

Experimental field-scale fires designed to measure turbulent flux at the fire–atmosphere interface can provide insights into near-surface atmospheric processes controlling fire behaviour. Sonic anemometry allows for the ability of measuring 3-dimensional

Received: 21 June 2022
Accepted: 28 October 2022
Published: 14 November 2022

Cite this:
Katurji M *et al.* (2022)
International Journal of Wildland Fire
doi:[10.1071/WF22100](https://doi.org/10.1071/WF22100)

© 2022 The Author(s) (or their employer(s)). Published by CSIRO Publishing on behalf of IAWF. This is an open access article distributed under the Creative Commons Attribution-NonCommercial-NoDerivatives 4.0 International License (CC BY-NC-ND)

OPEN ACCESS

wind velocity, air temperature and humidity at high sampling rate, and quantifying momentum, heat, and moisture fluxes between the fire and the overlying atmosphere. These experiments include *in situ* tower-mounted sonic anemometer measurements from spreading fires in low grass to higher canopy fuels (Clements et al. 2006, 2007; Heilman et al. 2019). Results from these experiments are then analysed in regards to quantifying the energy exchanged between the fire and the overlying atmosphere and the role of near-surface environmental shear and static stability on fire behaviour (Potter 2012). Other studies (Heilman et al. 2015, 2019) carried out measurements of vertically distributed turbulent heat and momentum flux during a surface fire progressing under 18–23 m high pine trees. Their results confirmed that the largest enhancement of vertical turbulent flux happens at or above canopy levels. Spectral analysis of momentum and heat flux suggested that fire-atmosphere interactions can happen across a wide range of frequencies, and further studies are needed to assess how those fluxes feedback into fire behaviour. Complex vegetation cover, including spatial density variations, forest gaps and edges, and steep topography will produce spatially complex turbulent interactions (Schlegel et al. 2012, 2015; Kiefer et al. 2018). The presence of dense vegetation acts to increase wind shear and the production of turbulent kinetic energy, reduce the mean wind speed and increase gusts, and enhance vertical motion allowing for an increase in downward momentum transfer from the atmospheric surface layer towards the fire (Schlegel et al. 2012, 2015; Kiefer et al. 2018).

The impact of atmosphere driven momentum surges on fire behaviour has not been extensively studied. For grass fires, we now can hypothesise that convective heating pulses originating from the flaming zone are responsible for fuel heating and could play a large role in fire spread in any direction along the fire line (Cunningham and Linn 2007). These processes have been modelled by coupled atmospheric fire large eddy simulation models like FIRETEC (Cunningham and Linn 2007) and observed in laboratory experiments (Finney et al. 2015; Tang et al. 2019). Turbulent flaming zone dynamics can now be observed using thermal image velocimetry (IV) techniques for real landscape scale experiments (Katurji et al. 2021), and have been shown to be related to overlying wind turbulence spectra. However, the role of downward momentum surges sourced from the ABL and their associated turbulence structures have not been studied in relation to fire horizontal convective heating dynamics, mainly because it is very difficult to measure these coupled scale dependent processes. In this paper, we present observations of atmospheric turbulence structures over a fast-spreading shrub fire and discuss their implication on fire behaviour. The methodology involves collecting *in situ* turbulence data from ultrasonic anemometers on towers up to 30 m AGL placed within an experimental burn. The data are then analysed to extract the population of turbulent sweep, ejection, inward and outward motion, which are then compared with observed fire sweeps

and their characteristics using IV and 2D convolution filters applied to the high-resolution aerial imagery. This research highlights the importance of multiplatform and multimodal observations, which included both *in-situ* point measurements and uncrewed aerial imagery to enable the analysis of coupled atmosphere–fire interactions.

Methodology

Experimental burn design

The experimental burn layout is shown in Fig. 1 and included four burn blocks hereafter referred to as plots P1, P2, P3, and P4. P5 and P6 are not included in this study due to the limited data obtained. The experiments were carried out on 2 and 6 March 2020 in the Rakaia Valley in New Zealand. Plots P3 and P4 were instrumented with two 30 m sonic anemometer towers shown in Fig. 1 with instrument details shown in Table 1. The two towers were nearly centred in the burn blocks while the fire line and flaming zone passed across. The analyses for plot P1 and P2 use meteorological data from the tower in plot P3.

Atmospheric turbulence analysis

Wavelet transform

Data de-spiking was carried out due to erroneous readings associated with extreme heat when flames touched the wind sensor. Sonic tilt and orientation corrections were also carried out on the sonic anemometer data, following the techniques outlined in Katurji et al. (2021), Seto et al. (2014), and Coen et al. (2004). The orientation of the plots were determined to be 22° west of True North for P1 and P2, and 43° west for P3 and P4. The streamwise (U) velocity component was then constructed from geometrically projecting the wind velocity on the 1-h mean wind direction for all the plots prior to the fire period. Wind speed perturbation values were calculated by subtracting the instantaneous wind speed from its 1-min rolling average.

This study used the python package PYCWT to calculate the wavelet transform for time frequency analysis. The package is based on Torrence and Compo (1998) and Grinsted et al. (2004) and has been used in various studies (Norel et al. 2021; Hunt and Zaz 2022). Unlike Fourier transform, wavelet transform reserves the temporal information alongside the frequency information and is more suitable to look at the temporal variations of coherent structures in the turbulence time series from the streamwise and vertical wind velocity.

In this work, the continuous wavelet transform is applied to the 20 Hz sonic tower data at different heights to investigate the coherent structures and spectral peaks and periods across different height levels and different experiments. The transform is done using the equation:

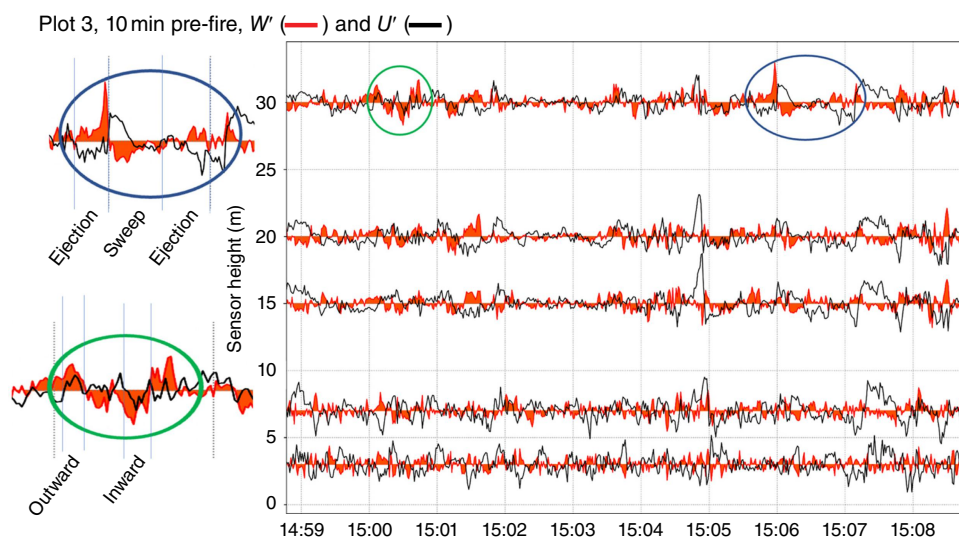
$$T_{\psi}(b, a) = \frac{1}{a^{\frac{1}{2}}} \int_{-\infty}^{\infty} \psi\left(\frac{t-b}{a}\right) f(t) dt \quad (1)$$



Fig. 1. Experimental burn layout showing plot sizes, fire spread overlay on plots, fire spread (red arrows) and other site pictures. The black letters in the top left picture represent the plots where fire breaks were carried out. The blue lines in the top left picture represent the planar field of view from a camera on an uncrewed aerial vehicle showing the top right picture. The charcoal hot box was used as a thermal reference for aerial infrared imagery (not used in the analysis in this paper). The 30 m tower setup and sonic anemometer, its thermal insulation, and state after the fire is shown in the bottom panels.

Table 1. Observational systems and corresponding measurement parameters and specifications.

Observational system	Instrument details	Measured variable	Installation details
Nadir visible video acquisition	Video camera on a DJI Ltd Phantom Video resolution 12 MP RGB	Visible video at 30 fps from nearly 200 m above ground level	On uncrewed aerial vehicle
In-fire wind turbulence towers in plots P3 and P4	Applied Technologies, Inc. 3-dimensional ultrasonic anemometer – SATI/3(K) series, Campbell Scientific CR6 datalogger K-probe – 150 mm vertical and horizontal measurement path length. Sampling frequency 20 Hz	U (+ve towards east), V (+ve towards north), W (+ve vertically upwards) [ms^{-1}]	3, 7, 15, 20, and 30 m AGL and perpendicular to fire line
Automatic weather station	Wind cup anemometer (model Vaisala Vector A101M) Wind vane (model Vaisala W200P) Air temperature and relative humidity sensor (model Campbell Scientific EE181) CR1000 data logger sampling at 1 min interval with 10 min averaging period	Wind speed [ms^{-1}] Wind direction [degree from bearing north] Temperature of air [$^{\circ}\text{C}$] and relative humidity [%]	Wind speed and direction measured at 10 m AGL Air temperature and relative humidity measured at 1.5 m AGL

**Fig. 2.** Vertical (W) and streamwise (U) velocity perturbations from the 30-m tower in plot P3. The variations in vertical (streamwise) velocity perturbations are between -1.8 and 2.1 ms^{-1} (-2.4 to 3.7 ms^{-1}). 20-Hz perturbations were calculated from a 1-min rolling average window and then subsampled with a 1 s window average. Examples of sweep, ejection, inward, and outward motions are extracted in the left panel.

where a , b is the scaling and translation parameter, respectively, and dt is the time step. Following previous studies applying the wavelet transform on sonic anemometer data (Kelley *et al.* 2000; Cava *et al.* 2017), the Morlet wavelet is used as the mother wavelet function (ψ).

Quadrant analysis

Wavelet transform can give temporal coherency information at different frequency scales, but the method cannot distinguish different types of turbulent coherent structures. These involve ‘ejection motion’ associated with turbulent eruption of low momentum streaks away from the surface; ‘sweep motion’ or deceleration of the flow caused by the turbulent motion towards the surface; ‘outward motion’ associated with the acceleration of the flow away from the surface

due to low-level convergence; and ‘inward motions’ associated with deceleration of the flow moving towards the surface due to low-level divergence (Christen *et al.* 2007; Li and Bou-Zeid 2011; Wallace 2016). The quadrant analysis in this study uses the instantaneous product of the streamwise velocity (U') and vertical velocity (W') perturbations. For momentum flux, sweeps would be $W' < 0$, $U' > 0$, ejections: $W' > 0$, $U' < 0$, outward motion: $W' > 0$, $U' > 0$, and inward motion: $W' < 0$, $U' < 0$ (a sample from the tower data is shown in Fig. 2).

Flaming zone observation and image velocimetry (IV)

IV was applied on uncrewed aerial vehicle (UAV) overhead fire videos following the methods described in Katurji *et al.* (2021)

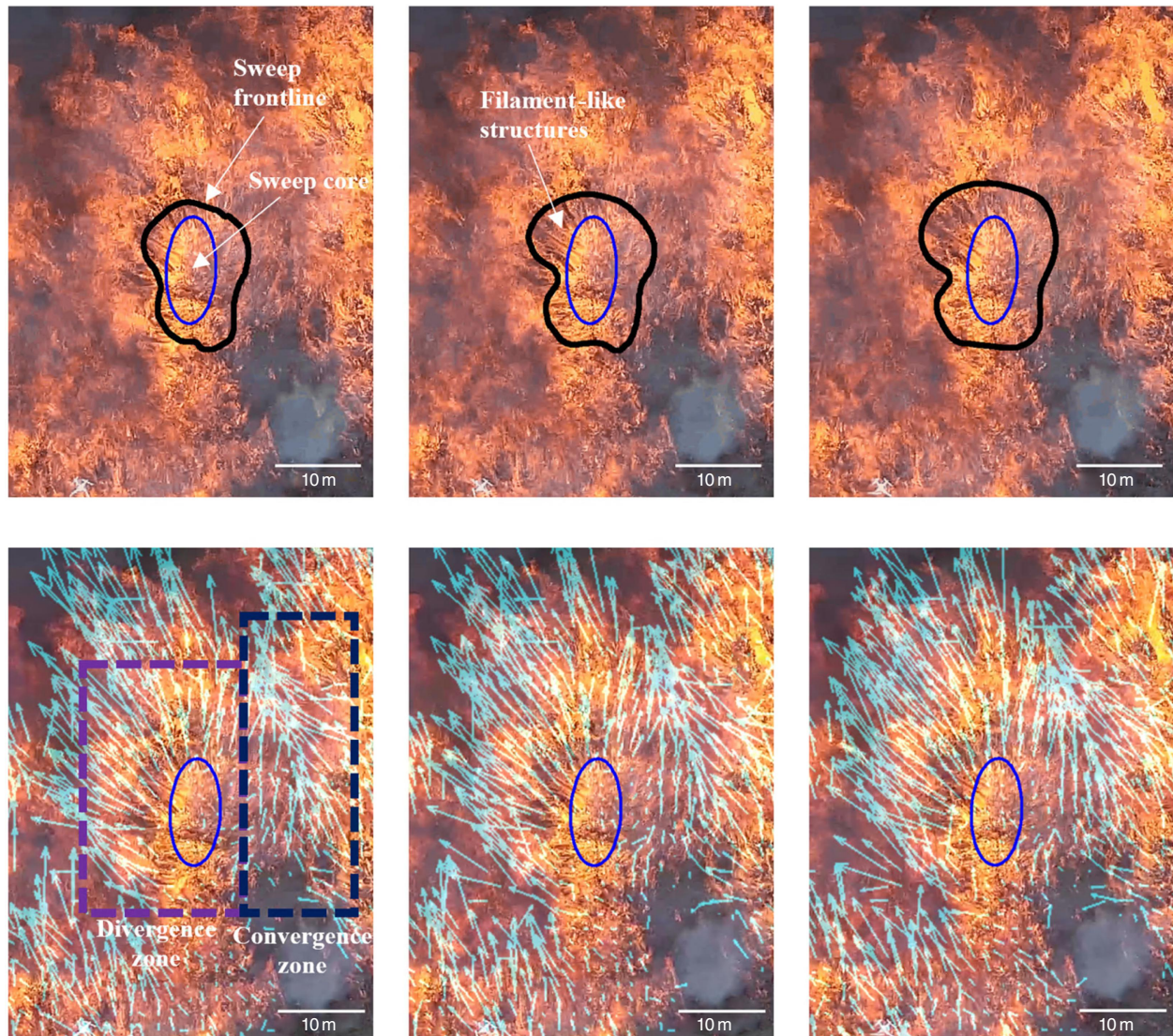


Fig. 3. Time sequenced (at 0.033 s interval) frames extracted from the UAV video recorded during the P2 burn (top) and an example of the resulting image velocimetry of identified fire sweep events (bottom). Blue vectors represent the observed motion of the fire obtained from image velocimetry. The sweep outline (black circle) was estimated based on a visual inspection of the horizontal radial streaks and their termination zone.

and in order to derive time varying spatial displacements of flame structures shown in Fig. 3. These structures manifest as diverging flame streaks that ignite downwind vegetation (example in Fig. 4b, c). The resulting vectors from the IV represent an estimation of the direction and magnitude of the displacement of the observed fire features between two consecutive frames that were acquired at 0.033 s intervals. It was found that the divergence of the fire flow outwards from a near static centre were successfully captured and represented using IV (a video of the flaming zone observations from plot P2 is provided in supplementary material video_flamingZone_P2.mp4). In this way, IV was used to develop a methodology capable of identifying fire sweeps and recording their durations from overhead UAV videos.

This post IV methodological step applies a 2D convolution on the displacement vector field, and uses a kernel designed to highlight the divergence of fire sweeps spatially and temporally. The kernel consists of a convolution matrix calibrated to capture a series of sweeps previously identified via visual inspection and is limited by the size of the flaming zone and obscuration of the smoke. Thresholding is then applied on the scalar fields to isolate the fire sweeps, which are then tracked frame by frame based upon their location and estimated size. The duration or residence time is estimated as the difference between the time of the initial frame and the final frame. This process is applied on all the displacement vectors, resulting in a 2D scalar field of divergence representing the likelihood of occurrence of fire sweeps.



Fig. 4. Observed flaming zone in plot P2 from nearly 200 m AGL using a UAV. Panels (b) and (c) cover the spatial area outlined in the white box in panel (a). The white lines in panels (b) and (c) represent the flame front at time of ignition plus 121.5 s. The black dotted outline in (b) and (c) shows the area of a fire 'sweep' and its impact on vegetation ignition. The black radial lines from panel (b) represent the direction of the flames emanating from the circumference of the fire sweep.

Results and discussion

Meteorological and burn conditions

P1 and P2 were conducted under a synoptically driven nor-wester wind regime that produced orographically channelled down-valley winds, and warmer and drier air conditions as the airflow descended from the New Zealand Southern Alps towards the Rakaia valley. Burn experiments for P3 and P4 occurred during a typical up-valley afternoon air flow causing fluctuation in air temperature reaching up

to 1.5°C and associated with the convective boundary layer (see third panel of Fig. 5). The burn durations for all plots varied between 3 and 5 min with an initial straight-line ignition and a wind driven flaming process. Fire behaviour and meteorological conditions are summarised in Table 2.

Wind turbulence spectra

For all the experimental burn plots, the smallest detectable period (derived from the last peak in the spectral power) of the turbulent wind velocity appears to get shorter as the

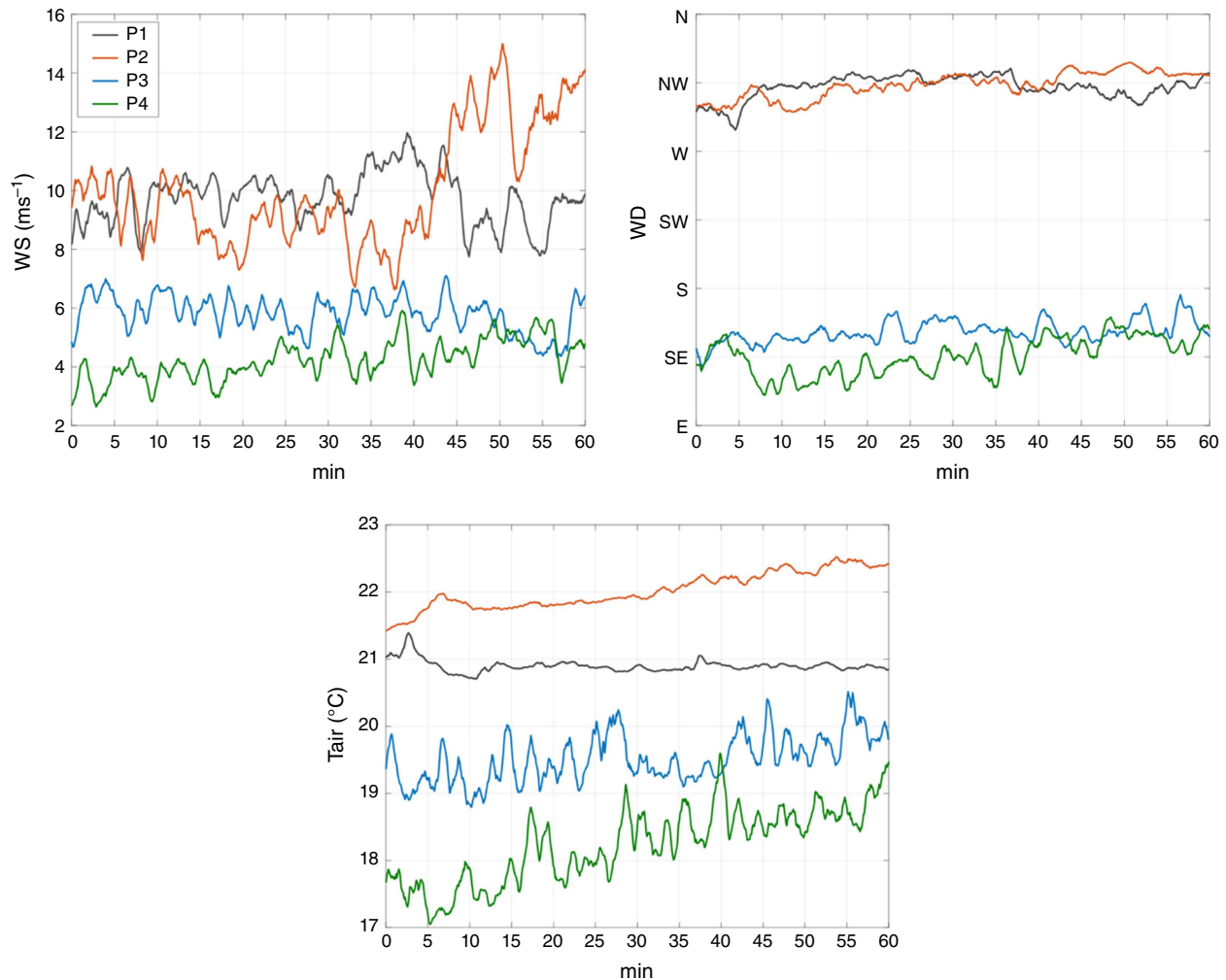


Fig. 5. Time series of wind speed (WS), wind direction (WD), and air temperature (Tair) for 1-h pre-fire at 30 m AGL and 1-min average interval. Plots P1, P2, P3, and P4 are shown in different colours. Due to different burn times and data availability, data for plots P1, P2, and P4 were from the tower in plot 3, while data for plot 3 were from the tower in plot 4.

measurement gets closer to the canopy (Fig. 6), which is expected as smaller turbulent length scales populate the wall-bounded boundary layer. The periods (or time scales) are presented by the local maxima in the spectral power and are highlighted by the horizontal dotted lines in Fig. 6. For heights less than 15 m, where the observed flame heights (between 3 and 6 m, Table 2) occurred, the results suggest that the smallest turbulent time scales with highest spectral power along the streamwise wind direction can occur between 3 s and 64 s. These results also show that the turbulent time scales vary between the atmospheric stability regimes of plots P1 and P2 compared to P3 and P4 where the longer time scales (3–96 s) were detected for the P3 and P4 meteorological conditions influenced by thermal circulation regimes as opposed to the stronger wind speed conditions of P1 and P2. This result is also reflected by the vertical wind spectra of P1 and P2 where shorter time scales were recorded (1–8 s) compared to P3 and P4 (4–128 s).

Atmospheric sweep, ejection, inward and outward motions

Atmospheric turbulent structures plotted against time for all the burn plot periods (Fig. 7) show more sweep and ejection events than inward and outward events. It has been previously suggested that coherent sweep (gust) and ejection (burst) motions dominate near-surface momentum and scalar fluxes (Li and Bou-Zeid 2011). The reduction of the number of inward and outward motions for P1 and P2 compared to P3 and P4 does support the earlier findings of the time scale difference between the shear driven surface layer condition of P1 and P2 and the thermally driven surface layer turbulent layer of P3 and P4. This conclusion is also supported by results from quadrant analysis from sonic anemometer towers in atmospheric boundary layers of non-fire applications (Christen *et al.* 2007). Forward slanting coherence of sweep and ejection structures (highlighted in yellow, Fig. 7) across the 30 m tower height may suggest that

Table 2. Experimental conditions including fire behaviour, fuel, and meteorological conditions (averaged over duration of burns) recorded from the weather station tower marked by a blue circle centred with 'x' in Fig. 1.

Plot	Ignition time (plot edge reached) [NZDT]	T _{air} [°C] (RH) [%]	Wind speed [ms ⁻¹] (direction) [°]	Mean gorse height [m]	Pre-burn total fuel load (gorse + grass + litter + debris) [kg m ⁻²]	Total fuel consumption [kg m ⁻²]	Rate of spread [m/s]	Flame height [m]
P1	02/03/2020, 10:10 (10:14)	20.7, (36)	8.27 (310)	0.83	3.4	2.5	0.89	4.9
P2	02/03/2020, 12:11 (12:14)	22.9, (33)	9.8 (311)	1.10	7.4	6.7	0.92	3.7
P3	06/03/2020, 15:08 (15:12)	21.6, (41)	6.8 (146)	0.84	3.4	2.4	0.9	5.4
P4	06/03/2020, 13:31 (13:36)	20.0, (43)	5.0 (142)	0.85	4.9	3.4	0.75	5.6

Flame heights were measured using measuring stakes and video imagery. Fuel loadings before and after the burns were measured using destructive sampling techniques from various mesh grids in the plots. Rate of spread was calculated from inspection of overhead video timing when the torching started and when the flame front reached the end of the plot (these were cross checked with observations from firefighters on the ground).

events can originate from within the surface layer (above the observed 30 m roughness boundary layer) and impinge on the surface, which is an area for future research. These types of interactions will have a time scale associated with them (the width of the black boxes) and the frequency of occurrence is shown and discussed in Fig. 8. These events can be significant as it is our hypothesis that fire 'sweeps', explained in the following section, can be impacted by these atmospheric turbulent structures by prolonging their duration and/or expanding the flame-vegetation interaction zone.

Fire sweeps

UAV overhead visible video of the gorse vegetation fire carried out in P2 and P4 was selected for this analysis. Fig. 3 highlights the observable flaming zone and some of its main features during the steady-state phase of the fire spread. The flaming zone dynamics were characterised by intermittent 'fire gusts' in which clusters of unburned fuel were covered by the fire and ignited. Fire gusts were typically accompanied by strong tilting of the flame front inducing, in most of the cases, direct flame impingement.

The structures in Fig. 3 are referred to as 'fire sweeps', and are characterised by divergent motion of fire (or 'fire sweep frontline', black line) from a nearly static luminous region (or a 'fire sweep core', region inside blue line). Structures with these characteristics were identified sporadically at multiple locations into the flaming zone. Generally, they were found to have a characteristic radius of ~10 m during the incipient stage up to ~20–30 m during its peak. The relative difference of luminosity between the core and the rest of the fire sweep can be attributed to an intensification of a thermal emission from soot incandescence inside the flame. Several studies in laboratory flames have shown that visible flame luminosity and thermal radiation tends to intensify with the availability of oxygen for combustion (White *et al.* 2017), suggesting that the reaction rate and consequently heat release rate inside fire sweep core is high relative to the rest of the fire sweep. The oxygenation process of the sweep core can be linked to a high local fuel concentration harmonised with the natural buoyant dynamics of the flaming zone. Within fire sweep cores, the mixture of oxygen and fuel is physically strengthened leading to a localised increase in combustion rates. Inspection of side-view UAV footage (not shown here) suggests that tilted flames from individual bushes located near the core region are at the origin of these structures. IV was used to derive and map the displacement of fire features during fire sweep events. A detailed inspection of the displacement vectors around fire sweeps revealed the existence of convergent zones located between two fire sweeps, as shown in Fig. 3.

As explained in the 'Flaming zone observation and image velocimetry (IV)' section, a 2D convolution algorithm was developed to track the number and duration of fire sweeps (for limited periods when smoke was not obscuring the

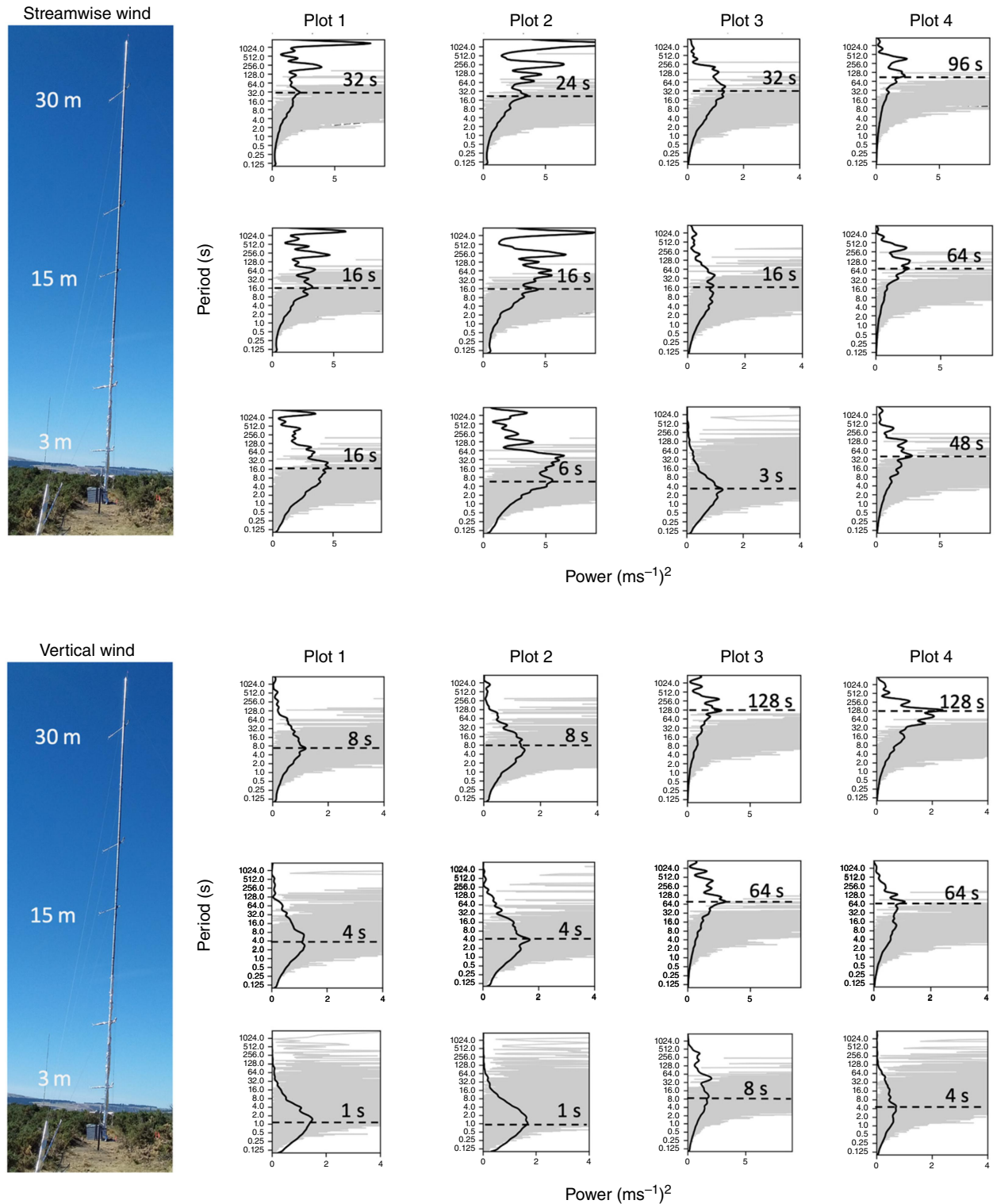


Fig. 6. Black line shows the time integrated spectra across the wavelet time frequency decomposition showing the period on the y-axis vs spectral power on x-axis for plots P1, P2, P3, and P4 and for three selected height levels on the tower (3, 15, and 30 m). One-hour pre-fire time series data from each plot were used to conduct this spectral analysis. The grey line shows the Fast Fourier decomposition inserted for reference but not used in the analysis. The horizontal dotted lines and the corresponding period is an estimate to where the smallest detectable period is before the power drops. Due to different burn times and data availability, data for plots P1, P2, and P4 were from the tower in plot P3, while data for plot P3 were from the tower in plot P4.

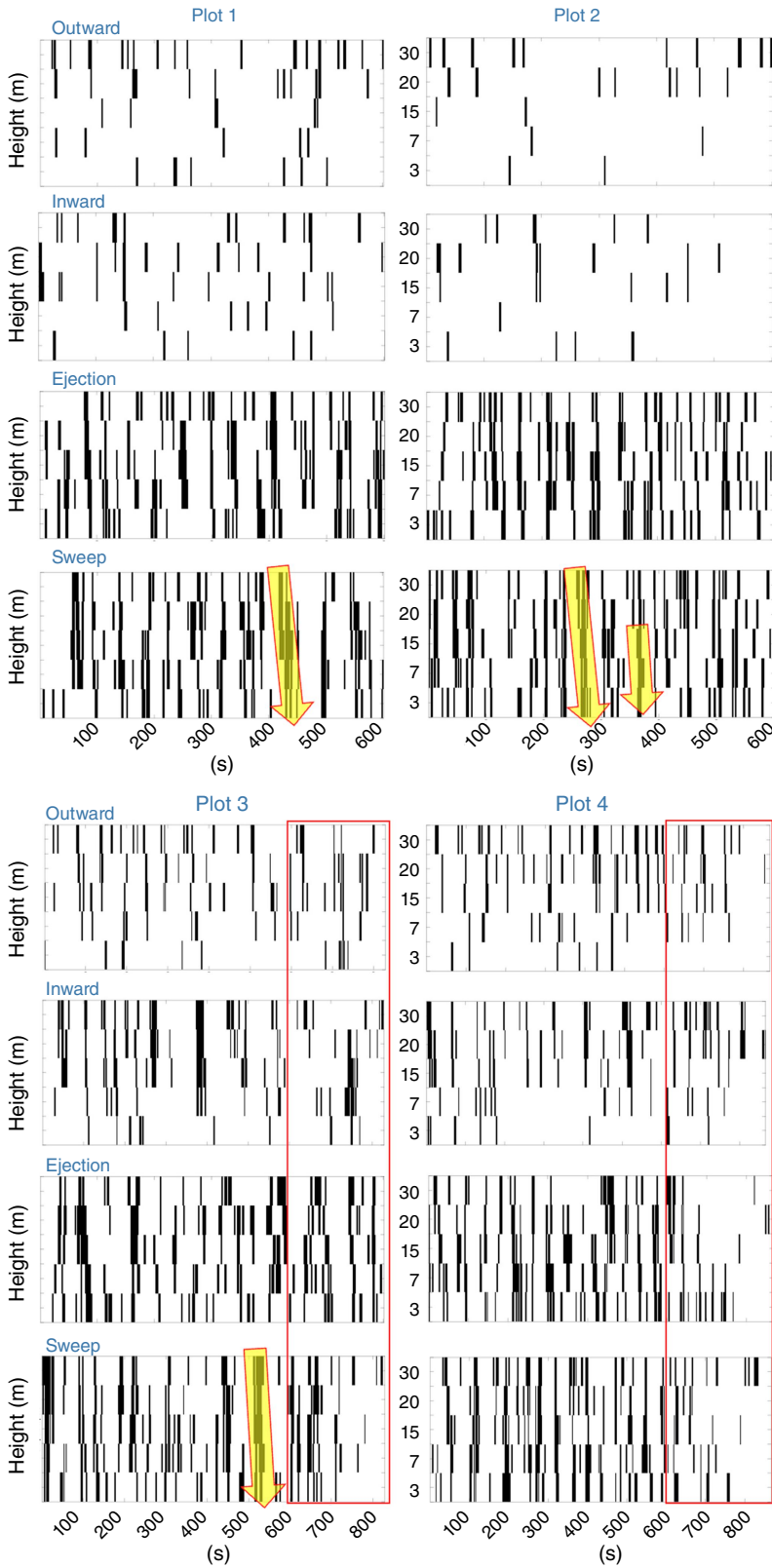


Fig. 7. Sweep, ejection, inward and outward events detected at all the five height levels of the *in situ* tower for plots P1, P2, P3 and P4. A sweep/ejection/inward/outward ‘instance’ is detected based on a the 20 Hz data following the methodology described in the ‘Quadrant analysis’ section, then an ‘event’ (represented graphically by the black bars) is logged if the ‘instance’ stay in a sweep/ejection/inward/outward category for 1 s or longer. The red outlined box shows the period when the fire was progressing through plots P3 and P4. The yellow arrows show examples of downwards propagating structures. Due to different burn times and data availability, data for plots P1, P2, and P4 were from the tower in plot P3. While data for plot P3 were from the tower in plot P4.

flames for plots P2 and P4). Two main groups of fire sweeps were identified. The first group is characterised by short-duration structures (< 1 s), generally quickly appearing and

disappearing sporadically with short displacement through the flaming zone. Fire sweeps of the second group presented longer durations (up to 6 s) and were observed to move

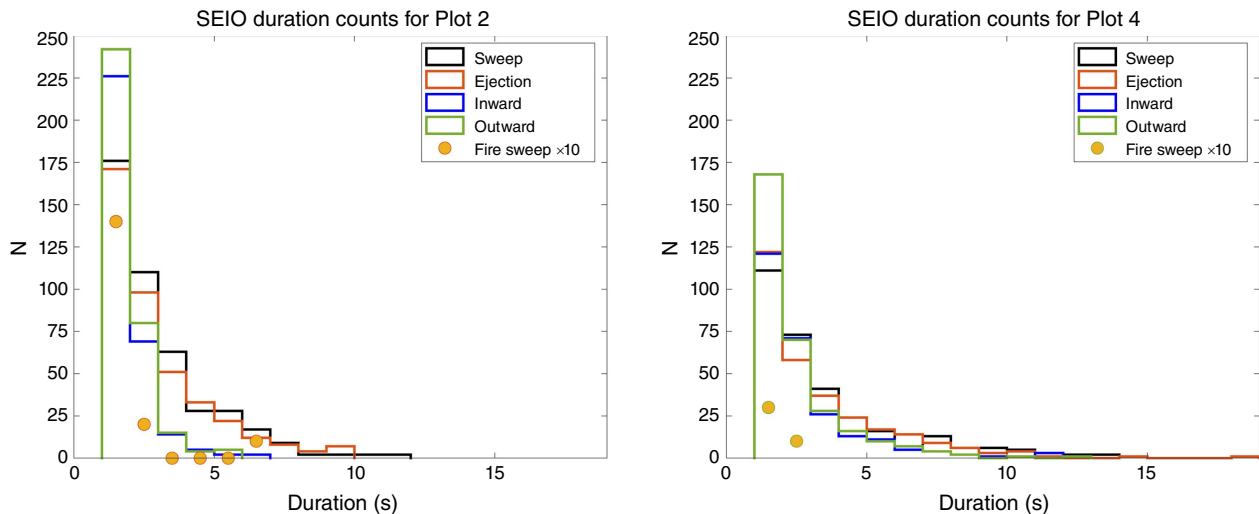


Fig. 8. Histogram of durations of atmospheric sweeps (S), ejection (E), inward (I) and outward (O) motions across all tower height level measurements (accumulated from 3 to 30 m). Fire sweep durations (number of occurrences multiplied by a factor of 10 to scale properly) from image velocimetry and 2D convolution algorithm are also inserted for plots P2 and P4. Due to different burn times and data availability SEIO data for plots P2 and P4 were from the tower in plot P3.

across the flaming zone, some of them from the back to the head of the fire. A statistical summary of fire sweep durations (calculated over a period of 27 s of fire progression for P2 and P4) is shown in Fig. 8 along with the duration of atmospheric coherent turbulent motion. Atmospheric sweeps and ejection occurred more frequently in P2 than P4, while the duration of inward and outward motions in P4 were slightly longer. The small number of occurrence of fire sweeps in P4 as compared to P2 is mainly attributed to the smoke levels (obscuring the visible detection of the flaming zone) that were very high in P4 as opposed to the better ventilated and higher wind speed conditions of P2 that makes the flames more visible. Nevertheless, the majority of the fire sweep durations were under 3 s with the expectation of the occurrence of a few at 6 s. The number counts of atmospheric and fire coherent turbulent structures are not expected to match as the quadrant analysis was done over 600 s pre-fire and the IV and 2D convolution tracking for 27 s during the fire progression.

Conclusion and discussion

Experimental burns provide unique observations on fire behaviour during specific meteorological conditions, vegetation fuel types and loading. Although we have developed some understanding of how fire-induced turbulence could modify the ambient flow field in the overlying roughness boundary layer, our understanding is still spatially limited and is largely due to the difficulty and analytical limitations of point measurements using sonic anemometer towers (e.g. Clements *et al.* 2006, 2007; Heilman *et al.* 2015). The use of high-speed thermal imagery video of a fire's flaming zone and derived IV techniques (Katurji *et al.* 2021) can help

in evaluating the kinematics of the flaming zone even at the turbulence scales. However, combined observations of wild-fire dynamics and atmospheric turbulence remains a challenge and we have largely depended on numerical modelling simulations for this purpose (e.g. Linn *et al.* 2012; Kiefer *et al.* 2018). This study focussed on combining for the first time measurements from a sonic anemometer tower placed inside or very close to an experimental wind driven fire and aerial visible video of the flaming zone. The analyses attempted to relate atmospheric coherent turbulent time scales and structures to fire sweeps observed within the flaming zone using the experimental burns carried out for gorse shrub fuels in the Rakaia valley, New Zealand. Observations included UAV based high resolution video from around 200 m above the spreading fire and 3D sonic anemometers from an in-fire 30 m tower. Due to different burn times and data availability the turbulent coherent structure analysis (sweep/ejection/inward/outward) for plots P1, P2 and P4 was from data from the tower in plot P3. The distance from tower 3 to any of the plot boundaries (with the exception of its own plot) varied between 100 and 400 m with homogenous upwind surface roughness conditions (gorse on the river bed). For the observed 15 and 30 m AGL meteorological conditions, we have derived the smallest characteristic turbulent length scale by assuming stationarity in turbulence distribution following Taylor's hypothesis (Taylor 1938), and using spectral data from Fig. 6 to be between 131 and 480 m, which acceptably overlaps with the tower separation distance to plots P1 and P2. While turbulence should not be considered stationary in complex boundary conditions at the fire-atmosphere interface, we will assume that measurements from tower 3 will represent the atmospheric conditions for the rest of the plots.

A point-based statistical technique previously used for deriving atmospheric coherent turbulent motion over vegetated canopies (Li and Bou-Zeid 2011; Wang et al. 2013; Wallace 2016), and more recently applied for experimental fire observations (Heilman et al. 2021) was employed to characterise the number, duration, and type of turbulence in the ambient flow field. The characteristic time scales of pre-fire ambient turbulence varied between 1 and 128 s. Pre-fire atmospheric turbulent structure analysis suggests that the roughness boundary layer (a few vegetation heights aboveground level) is a critical medium within which atmospheric sweeps reaching durations up to 10 s have the potential of impinging on the fire front. This result should not be confused with the conditions during or after the fire front passage where changes in the distribution of atmospheric coherent turbulent structures are expected. For example, observations from Heilman et al. (2021) suggest that fire-induced turbulence can result in upward momentum and heat transfer that reduces the number distribution of sweeps and ejections normally associated with shear driven flows. Our data were not statistically significant to support Heilman et al. (2021) for conditions during and after the fire front passage.

The flaming zone dynamics were well captured by the aerial videos, and new IV techniques building on Katurji et al. (2021) were employed to derive their advection velocity. Results showed the time evolving nature of a fire sweep that occurred regularly across the flaming zone with durations varying between 1 and 7 s. The population statistics of fire sweeps were compared to the derived atmospheric coherent turbulent structures from the quadrant analysis technique. Although the number of detected fire sweeps were less than the number of atmospheric structures due to smoke obscuring the flaming zone and impacting the image quality for analysis, the durations of the fire sweeps do match with the shorter atmospheric turbulence structures (< 3 s) with a small number of fire sweeps extending between 6 and 7 s.

Further analysis is needed to investigate coupled atmosphere–fire energy flux interactions such as the quantification of intensity and direction of fluxes as a function of coherent structures following techniques presented in this study and Heilman et al. (2021). The observational and analytical methods employed in this research such as atmospheric turbulence structure characterisation, IV and feature tracking of fire sweeps that built on the methods described in Katurji et al. (2021), can provide a comprehensive toolkit when investigating coupled atmosphere–fire interactions from observations as well as from simulations using Large Eddy Simulation (LES) models.

Supplementary material

Supplementary material is available [online](#).

References

- Bebieva Y, Oliveto J, Quaife B, Skowronski NS, Heilman WE, Speer K (2020) Role of Horizontal Eddy Diffusivity within the Canopy on Fire Spread. *Atmosphere* 11(6), 672. doi:10.3390/atmos11060672
- Cava D, Mortarini L, Giostra U, Richiardone R, Anfossi D (2017) A wavelet analysis of low-wind-speed subscale motions in a nocturnal boundary layer. *Quarterly Journal of the Royal Meteorological Society* 143(703), 661–669. doi:10.1002/qj.2954
- Christen A, van Gorsel E, Vogt R (2007) Coherent structures in urban roughness sublayer turbulence. *International Journal of Climatology* 27(14), 1955–1968. doi:10.1002/joc.1625
- Clements CB, Potter BE, Zhong S (2006) *In situ* measurements of water vapor, heat, and CO₂ fluxes within a prescribed grass fire. *International Journal of Wildland Fire* 15(3), 299–306. doi:10.1071/WF05101
- Clements CB, Zhong S, Goodrick S, Li J, Potter BE, Bian X, et al. (2007) Observing the Dynamics of Wildland Grass Fires: FireFlux—A Field Validation Experiment. *Bulletin of the American Meteorological Society* 88(9), 1369–1382. doi:10.1175/BAMS-88-9-1369
- Coen J, Mahalingam S, Daily J (2004) Infrared Imagery of Crown-Fire Dynamics during FROSTFIRE. *Journal of Applied Meteorology and Climatology* 43(9), 1241–1259. doi:10.1175/1520-0450(2004)043<1241:IIOCDD>2.0.CO;2
- Cunningham P, Linn RR (2007) Numerical simulations of grass fires using a coupled atmosphere–fire model: Dynamics of fire spread. *Journal of Geophysical Research: Atmospheres* 112(D5), D05108. doi:10.1029/2006jgd007638
- Finney MA, Cohen JD, Forthofer JM, McAllister SS, Gollner MJ, Gorham DJ, et al. (2015) Role of buoyant flame dynamics in wildfire spread. *Proceedings of the National Academy of Sciences* 112(32), 9833–9838. doi:10.1073/pnas.1504498112
- Grinstead A, Moore JC, Jevrejeva S (2004) Application of the cross wavelet transform and wavelet coherence to geophysical time series. *Nonlinear Processes in Geophysics* 11(5/6), 561–566. doi:10.5194/npg-11-561-2004
- Heilman WE, Clements CB, Seto D, Bian X, Clark KL, Skowronski NS, Hom JL (2015) Observations of fire-induced turbulence regimes during low-intensity wildland fires in forested environments: implications for smoke dispersion. *Atmospheric Science Letters* 16(4), 453–460. doi:10.1002/asl.581
- Heilman WE, Bian X, Clark KL, Zhong S (2019) Observations of Turbulent Heat and Momentum Fluxes During Wildland Fires in Forested Environments. *Journal of Applied Meteorology and Climatology* 58, 813–829. doi:10.1175/jamc-d-18-0199.1
- Heilman WE, Banerjee T, Clements CB, Clark KL, Zhong S, Bian X (2021) Observations of Sweep–Ejection Dynamics for Heat and Momentum Fluxes during Wildland Fires in Forested and Grassland Environments. *Journal of Applied Meteorology and Climatology* 60(2), 185–199. doi:10.1175/jamc-d-20-0086.1
- Hunt KMR, Zaz SN (2022) Linking the North Atlantic Oscillation to winter precipitation over the Western Himalaya through disturbances of the subtropical jet. *Climate Dynamics* doi:10.1007/s00382-022-06450-7
- Katurji M, Zhang J, Satinsky A, McNair H, Schumacher B, Strand T, et al. (2021) Turbulent Thermal Image Velocimetry at the Immediate Fire and Atmospheric Interface. *Journal of Geophysical Research: Atmospheres* 126(24), e2021JD035393. doi:10.1029/2021jd035393
- Kelley ND, Osgood RM, Bialasiewicz JT, Jakubowski A (2000) Using Wavelet Analysis to Assess Turbulence/Rotor Interactions. *Wind Energy* 3(3), 121–134. doi:10.1002/we.33
- Kiefer MT, Zhong S, Heilman WE, Charney JJ, Bian X (2018) A Numerical Study of Atmospheric Perturbations Induced by Heat From a Wildland Fire: Sensitivity to Vertical Canopy Structure and Heat Source Strength. *Journal of Geophysical Research: Atmospheres* 123, 2555–2572. doi:10.1002/2017jd027904
- LeMone MA, Angevine WM, Bretherton CS, Chen F, Dudhia J, Fedorovich E, et al. (2019) 100 Years of Progress in Boundary Layer Meteorology. *Meteorological Monographs* 59, 9.1–9.85. doi:10.1175/amsmonographs-d-18-0013.1
- Li D, Bou-Zeid E (2011) Coherent Structures and the Dissimilarity of Turbulent Transport of Momentum and Scalars in the Unstable Atmospheric Surface Layer. *Boundary-Layer Meteorology* 140(2), 243–262. doi:10.1007/s10546-011-9613-5

- Linn RR, Canfield JM, Cunningham P, Edminster C, Dupuy J-L, Pimont F (2012) Using periodic line fires to gain a new perspective on multi-dimensional aspects of forward fire spread. *Agricultural and Forest Meteorology* **157**, 60–76. doi:10.1016/j.agrformet.2012.01.014
- Norel M, Kałczyński M, Pińskwar I, Krawiec K, Kundzewicz ZW (2021) Climate Variability Indices—A Guided Tour. *Geosciences* **11**(3), 128. doi:10.3390/geosciences11030128
- Potter BE (2012) Atmospheric interactions with wildland fire behaviour – I. Basic surface interactions, vertical profiles and synoptic structures. *International Journal of Wildland Fire* **21**(7), 779–801. doi:10.1071/WF11128
- Schlegel F, Stiller J, Bienert A, Maas H-G, Queck R, Bernhofer C (2012) Large-Eddy Simulation of Inhomogeneous Canopy Flows Using High Resolution Terrestrial Laser Scanning Data. *Boundary-Layer Meteorology* **142**(2), 223–243. doi:10.1007/s10546-011-9678-1
- Schlegel F, Stiller J, Bienert A, Maas H-G, Queck R, Bernhofer C (2015) Large-Eddy Simulation Study of the Effects on Flow of a Heterogeneous Forest at Sub-Tree Resolution. *Boundary-Layer Meteorology* **154**(1), 27–56. doi:10.1007/s10546-014-9962-y
- Seto D, Strand TM, Clements CB, Thistle H, Mickler R (2014) Wind and plume thermodynamic structures during low-intensity subcanopy fires. *Agricultural and Forest Meteorology* **198–199**, 53–61. doi:10.1016/j.agrformet.2014.07.006
- Stull RB (1988) ‘An introduction to boundary layer meteorology.’ (Springer Science & Business Media)
- Sun R, Krueger SK, Jenkins MA, Zulauf MA, Charney JJ (2009) The importance of fire–atmosphere coupling and boundary-layer turbulence to wildfire spread. *International Journal of Wildland Fire* **18**(1), 50–60. doi:10.1071/wf07072
- Tang W, Finney M, McAllister S, Gollner M (2019) An Experimental Study of Intermittent Heating Frequencies From Wind-Driven Flames. *Frontiers in Mechanical Engineering* **5**, 34. doi:10.3389/fmech.2019.00034
- Taylor GI (1938) The spectrum of turbulence. *Proceedings of the Royal Society of London. Series A - Mathematical and Physical Sciences* **164**, 476–490. doi:10.1098/rspa.1938.0032
- Torrence C, Compo GP (1998) A Practical Guide to Wavelet Analysis. *Bulletin of the American Meteorological Society* **79**(1), 61–78. doi:10.1175/1520-0477(1998)079<0061:APGTWA>2.0.CO;2
- Wallace JM (2016) Quadrant Analysis in Turbulence Research: History and Evolution. *Annual Review of Fluid Mechanics* **48**(1), 131–158. doi:10.1146/annurev-fluid-122414-034550
- Wang L, Li D, Gao Z, Sun T, Guo X, Bou-Zeid E (2013) Turbulent Transport of Momentum and Scalars Above an Urban Canopy. *Boundary-Layer Meteorology* **150**(3), 485–511. doi:10.1007/s10546-013-9877-z
- White JP, Verma S, Keller E, Hao A, Trouvé A, Marshall AW (2017) Water mist suppression of a turbulent line fire. *Fire Safety Journal* **91**, 705–713. doi:10.1016/j.firesaf.2017.03.014

Data availability. The observation data used in this study can be shared upon request with the corresponding author.

Conflicts of interest. The authors declare no conflicts of interest.

Declaration of funding. This research was co-funded by the Ministry of Business, Innovation and Employment (MBIE), New Zealand, grant number C04X1603 and C04X2103, and the Royal Society of New Zealand (Grant No. RDF-UOC1701).

Acknowledgements. We thank all field support teams including technical and general staff. We also thank the landowner for their various contributions leading to the success of the field campaigns. The University of Canterbury atmospheric research team acknowledges the very thoughtful, well organised, and proactive support we have received from all the volunteering firefighting crew. The success of our experiments and the safety of our science crew can only be partially attributed to our design but greatly attributed to the safe and well-executed plan from the volunteer crew. A special thanks to the Scion UAV crew: Robin Hartley and Peter Massam.

Author affiliations

^ASchool of Earth and Environment, University of Canterbury, Christchurch, New Zealand.

^BNew Zealand Forest Research Institute, Scion, Rotorua, New Zealand.

^CDepartment of Civil and Natural Resources Engineering, University of Canterbury, Christchurch, New Zealand.

^DEarth Observation Data Centre GmbH, Franz-Grill-Straße 9, 1030 Vienna, Austria.

^EFire Emergency New Zealand- FENZ, Wellington, New Zealand.